

Figure 2: Best fit to the available photometry of Oph 2320.8–1721. The data points correspond from left to right to the following filters: R, I, J, H, K, L', ISOCAM LW1, ISOCAM LW4, and N. The solid line includes the contributions from the photosphere and the circumstellar excess, with the dotted line being the photospheric contribution alone. Both curves include a foreground reddening of $A_V = 10$ mag.

years, and keeps below the stellar limit provided that the object is younger than 15 million years, which is more than the expected lifetime of an embedded cluster and several times the estimated age of the ρ Ophiuchi cluster. The circumstellar excess, characterised by a spectral index $n = -1.6$ (where $n = -3$ would correspond to a central source without circumstellar material and $n > 0$ to a protostar totally embedded in its envelope) further supports the youth of Oph 2320.8–1721. The required foreground extinction to produce a good fit is $A_V = 10$ mag, much less than the average extinction, $A_V \sim 50$, deduced from CO maps of the area, suggesting that Oph 2320.8–1721 is placed near the front edge of the cloud. The effective temperature of the object, $T = 2650$ K, is

consistent with the spectral features discussed by Williams et al. (1995). On the other hand, due to the deuterium burning phase which Oph 2320.8–1721 is presumably undergoing, its age is practically unconstrained by our fits.

The long baseline in wavelength available with the new measurements, plus the insensitivity of the fit to the assumed age, make the above estimates much more robust than the ones presented in previous stages of this work. A significantly larger mass exceeding the stellar limit, implying a greater luminosity, would require a substantial increase in the amount of foreground extinction, which would be incompatible with the detection of the object in R. Moreover, this would decrease the required amount of circumstellar excess, making it inconsistent

with the rather flat shape of the $\log(\nu f_\nu)$ curve at longer wavelengths. New, high signal-to-noise spectra of Oph 2320.8–1721 in the H and K regions obtainable in the near future with SOFI at the NTT would help to further constrain the surface temperature and gravity of this object, thus giving independent estimates of its temperature and luminosity. In the meantime, however, we can say that the identification of Oph 2320.8–1721 as a young brown dwarf is already supported by a very considerable amount of observational material.

Acknowledgements: We wish to thank Jason Spyromilio for making a part of his service observing time at the NTT available to us, as well as to the ESO staff providing support to the observations at the NTT and the 2.2-m telescope. Based on observations with ISO, an ESA project with instruments funded by ESA Member States (especially the PI countries: France, Germany, the Netherlands and the United Kingdom) with the participation of ISAS and NASA.

References

- Adams, F.C., Lada, C.J., Shu, F.H., 1987, *ApJ*, **312**, 788.
 Allard, F., Hauschildt, P.H., 1995, *ApJ*, **445**, 433.
 Burrows, A., Hubbard, W.B., Saumon, D., Lunine, J.I., 1993, *ApJ*, **406**, 158.
 Calvet, N., Hartmann, L., Strom, S.E., 1997, *ApJ*, **481**, 912.
 Comerón, F., Rieke, G.H., Burrows, A., Rieke, M.J. 1993, *ApJ*, **416**, 185.
 Comerón, F., Rieke, G.H., Rieke, M.J., 1996, *ApJ*, **473**, 294.
 D'Antona, F., Mazzitelli, I., 1994, *ApJS*, **90**, 467.
 Lada, C.J. Adams, F.C., 1992 *ApJ*, **393**, 278.
 Mathis, J.S., 1990, *ARA&A*, **28**, 37.
 Rebolo, R. (ed.), 1997, "Brown dwarfs and extrasolar planets", ASP Conf. Series, in press.
 Rieke, G.H., Lebofsky, M.J., 1985, *ApJ*, **228**, 618.
 Rieke, G.H., Rieke, M.J., 1990, *ApJ*, **362**, L21.
 Williams, D.M., Comerón, F., Rieke, G.H., 1995, *ApJ*, **454**, 144.

F. Comerón
 fcomeron@eso.org

PMS Binaries in Southern Molecular Clouds Observed with ADONIS + COMIC

J.-L. MONIN and H. GEOFFRAY

Laboratoire d'Astrophysique – Observatoire de Grenoble, France

1. Introduction

The process of low-mass star formation is now well known for producing a large fraction of binary and multiple systems. This result is confirmed by many surveys (e.g. Reipurth & Zinnecker, 1993; Ghez et al., 1993; Leinert et al., 1993), showing that most, if not all, the

T Tauri stars (TTS) have companions. Therefore, the study of Pre-Main-Sequence (PMS) binary systems appears as a crucial key in understanding the process of star formation. However, due to the increasing number of multiple systems at small projected separations, the basic data do not exist for most of the individual members of these sys-

tems because of the limited angular resolution of the available instruments (cameras, spectrographs, and polarimeters), or the limited signal-to-noise ratio of the observations. For instance, some observations of PMS binaries have already been performed in Speckle at $2.2 \mu\text{m}$ (Ghez et al., 1993), but this was mainly for a study of the binary-star fre-

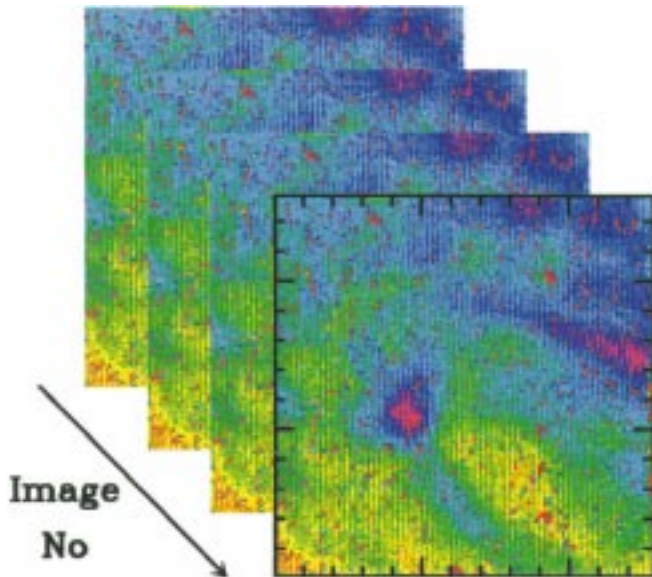


Figure 1: Example of successive (128×128) image planes recorded in the L band alternatively on the source (ON chopping mirror position) and on the nearby sky (OFF chopping mirror position). The image pattern is dominated by the sky + telescope + instrument thermal background emission, with a large amplitude of several thousands ADU over the image; no source is visible in the images at this point of the data reduction process. North is to the right, east down. Field of view is 4.6 arcsec.

quency and above all, the speckle observations do not provide such a high dynamical range as adaptive optics does.

The bulk of the emission from TTS peaks in the near-infrared. The 1–5 μm range is therefore particularly well suited for studying the Spectral Energy Distribution of such objects and estimate their luminosity and temperature. Indeed, the recent availability of a 3–5 μm window provided by COMIC allows to measure IR excesses at a high angular resolution, thus giving access to circumstellar accretion disks. Moreover, the separation distribution of PMS binaries peaks at ≈ 50 AU, corresponding to an angular separation of $\approx 0.3''$ at the nearest star-forming region observable from ESO La Silla.

The availability of the instrument ADONIS + (SHARP / COMIC), which allows to obtain images with a resolution down to ≈ 0.2 arcsec or less in the range 1 to 5 μm (J, H, K, L and M bands), with a field of view of the order of 10 arcsec, therefore provides a unique opportunity to study the binarity among PMS TTS. In practice, binaries with linear projected distance from 1500 AU down to 30 AU at the ρ Oph cloud distance, can be resolved and imaged with a high signal-to-noise ratio. At such a distance, images can be obtained of binaries with companion stars separated by less than the canonical predicted size of an accretion disk (≈ 100 AU).

We have started a series of observations of PMS binary systems in order to study the precise photometry of the binary components from 1 to 5 μm in these – often recently discovered – binary systems. From these measurements we will characterise the stellar Spectral Energy Distribution (SED) of the primary and its companion, adjust a blackbody model to estimate their luminosities and temperature, hence

masses and ages through the use of an HR diagram. At the same time, we will study the distribution of the circumstellar and circumbinary environment of our PMS targets, in order to study how the eventual left-over material is distributed after contraction.

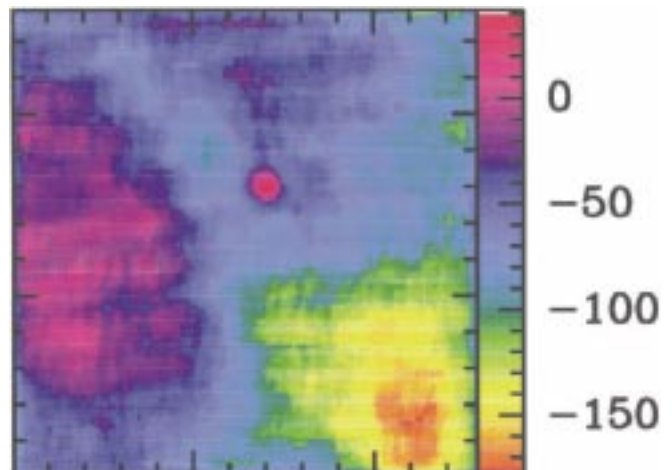
In this paper, we report on preliminary results of an observing run that took place in May 1996 and was the first scientific observing run with COMIC. We give some details of the observing procedure with COMIC at 3 and 5 μm , which appears non trivial because of the high level of thermal emissivity of the close instrumental environment in these wavebands. We compute an on-the-spot estimation of the limiting magnitude that one can hopefully attain at L and M. We present some images and SEDs that have been obtained. The complete results of this work will be presented in a forthcoming paper.

2. Observations

We have used ADONIS + COMIC on 3 nights in 1996, May 1 and 2 and May

5. The weather was excellent during the overall run and the experiment ran smoothly during its first scientific run, thanks to the help of the ADONIS team. From the adaptive optics point of view, TTS represent a tough challenge for the correction system since they are often dimmer than $V = 12$ and most interesting objects are often around $V = 14$. We have benefited from a new quadrant of the ADONIS EBCCD and we have been able to close the loop on the primary (i.e. brighter) component of all our sources, even one with a magnitude as high as $V = 14.9$ in the literature (V 536 Aql, Herbig and Bell, 1988). Every source was observed using the primary as a reference star. This solution appeared to work correctly for most of our objects since there was high enough a magnitude difference Δm between the primary and its companion. We had some correction problems only once, on a source with a Δm too close to zero. In such a case, the use of a numerical filter allows to reject the signal from the close companion and to restore a good correction. We also observed PSF reference stars every other observation, i.e. within 5 or 10 minutes on the average. These PSF measurements will be used as deconvolution calibrators to study the presence of dim circumstellar environment around our objects. We also observed photometric calibration stars every hour or so, so that we were able to determine the absolute photometry of both components in all the observed systems. We used approximately the same integration times in the JHK bands (during SHARP observations) and LM bands (COMIC observations). The large integration capacity of the COMIC detector allowed integration times as high as 10 seconds in L and 6 seconds in M. In fact, we always adjusted the integration time to get approximately half of the saturation level in the detector. In this configuration, the read-out noise is limited by the sky background statistical noise and the detector can be considered as perfect. The long integration times are not essential

Figure 2: Residual close instrumental background emission pattern after ON-OFF subtraction. The sky background contribution has been subtracted and the source is now visible, approximately in the middle of the image. The amplitude of the residual background pattern is only a few tens of ADU (scale at the right of the image). Same orientation and scale as Figure 1.



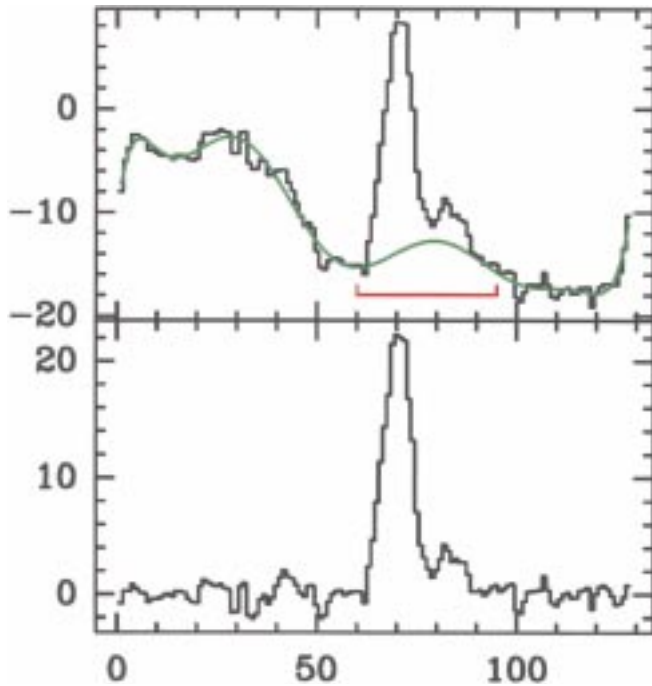


Figure 3: Line-by-line residual background fitting and subtraction. Upper panel: the source can be seen superimposed on the background. This background signal is fitted as a polynomial function (green line) outside the source position (red window). The lower panel shows the source and its companion after background subtraction. The residual rms noise is of the order of 1 ADU.

from the signal-to-noise point of view but are very convenient to increase the acquisition efficiency (integration time compared to read-out time).

3. Some Hints for High Background COMIC Data Reduction

The ADONIS bench allows us to use a tilt mirror to measure the sky emission on a nearby position. Three choices are possible.

(1) no chopping: then one has to move the telescope to measure the sky emission. This is slow and we didn't use it.

(2) simple chopping: the mirror moves every few images to allow the camera to measure the sky emission. This allows us to measure the sky emission if there is no sky emission gradient. The main inconvenient of this method is that the close environment thermal emission pattern changes between the ON and OFF position of the mirror. As a consequence, the sky emission is correctly suppressed in the ON-OFF operation but a new (lower) background pattern appears. This effect is well known in thermal infrared imaging and requires a beam-switching technique (nodding) to be cancelled. However, the ADONIS bench has been mainly designed for visible and "optical" near infrared (1–2.5 μm) observations, and beam-switching is not currently available. To cancel this effect, a solution consists of storing images of an empty part of the sky and record the close environment thermal emission pattern, in order to subtract it later from the observations. Unfortunately, we didn't measure such a pattern during our observations and we only used the simple chopping mode on all our sources. This obliged us to estimate *a posteriori* the "baseline" background in every image after pre-processing with the ECLIPSE package.

(3) double chopping: the mirror moves successively to ON, OFF1, OFF2 positions in order to measure the sky background emission on two symmetrical positions around the star. This allows us to remove any sky emission gradients, but doubles the close environment emission problem and we do not recommend to use it. Clearly, the double chopping cannot replace the beam-switching. Note that for extended sources where the close background baseline emission cannot easily be disentangled from the source emission, the use of the simple chopping appears mandatory, and it is also required to measure the thermal emission pattern of the close warm environment by performing a long enough integration (with simple chopping) on an empty part of the sky. Contrary to the sky

background emission that varies on short times, the close instrumental environment emission is relatively stable (as is its temperature) and does not need to be measured very often.

Data reduction has been performed using the ECLIPSE package developed by N. Devillard at ESO (Devillard, 1997), and some other classical data reduction packages (GRAPHIC and CLASS, two softwares developed in the Grenoble Observatory, and also IRAF).

We have removed the residual background pattern in our images by fitting a polynomial baseline on every line of the image. We found that this was more efficient than trying to fit a 2-D surface on the overall image. In any case, this implies that one defines some part of the image or line where the fit procedure must ignore the signal. We illustrate these various operations in Figures 1 to 3.

4. On Sky Performances

We have used our data to estimate the image quality and the limiting magnitude one can attain in the L and the M bands. Figure 4 shows the image of a binary (V 536 Aql, Monin et al., 1997), together with its associated PSF reference star, obtained with COMIC in the L band. The images have been flat-fielded and corrected for bad pixels, but no deconvolution was applied. The image correction was incomplete, but two diffraction rings can be seen on the object and on the PSF, and the correction errors are the same on both images. Photometric measurements are already possible, and deconvolution will provide a clean image of the binary. The L magnitude of the primary and the secondary are 7.1 and 8.2 respectively, and the separation of the binary is 0.5". These observations have been obtained with

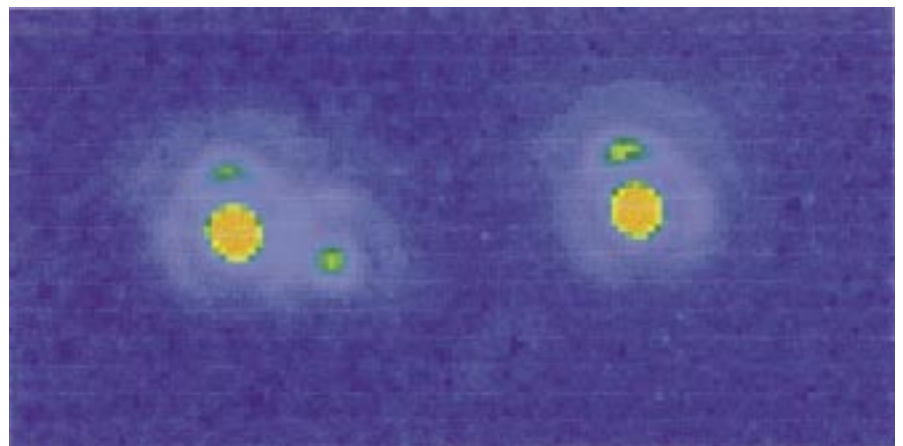


Figure 4: V536 Aql (left, $L_A = 7.1$, $L_B = 8.2$) image in the L band together with the PSF reference star (right). Two diffraction rings are visible both on the main component of the binary on the right part of the image and on the PSF. One diffraction ring is visible around the dim secondary of V536 Aql (the projected separation is 0.5" at P.A. 17°). North is to the right, east is down, and each image field of view is 2.2". Note that the correction errors have not been "CLEANed" and are the same on the object and on the reference star. As an example, the small bright feature in the first diffraction ring on top of each source (main component and psf, to the West) is an artifact.

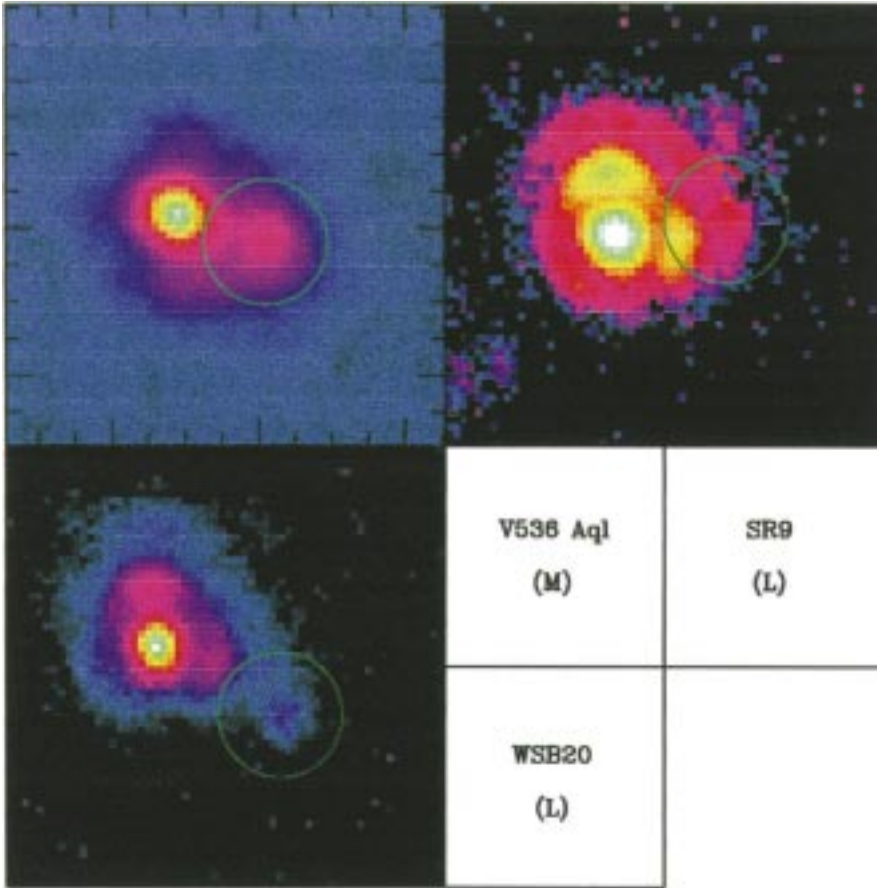


Figure 5: Sample images of close PMS binaries (V536 Aql, sep. $0.5''$, SR9, sep. $0.6''$, WSB20, sep. $0.7''$). The orientation (north to the right and east down) and the image scale (field of view of $2.2''$) are the same as in Figure 4. The respective name of the sources together with the corresponding IR photometric band are indicated in the figure. In every image, the circle traces the first diffraction ring around the secondary component.

an integration time per frame of 8–10 second and the total integration time is of the order of 30 s. We have estimated the limiting magnitude in the L band by comparing the background noise in the image with the amplitude of the signal on a photometric reference star.

On HR 4523 ($L = M = 3.3$), we obtain $L_{\text{lim}}(1 \text{ s}, 1 \sigma) = 11$. Marco et al. (1997) have computed the theoretical limiting performances of the COMIC camera from laboratory measurements at (900 s, 5σ). If we scale their results to (1 s, 1σ), we find $L_{\text{lim}} = 11.9$. These two estimates have been obtained with completely different methods and appear very consistent. In the M band on the same reference star, we obtain a limiting magnitude of the order of $M_{\text{lim}} = 8$. This is a bit smaller than the theoretical estimates of Marco et al. (1997) and can be explained by

(1) the fact that we have observed in M with the objective optimised for JHK which gives a resolution of $0.036''/\text{pixel}$, similar to that of SHARP1, but which oversamples the image in M (Lacombe et al., 1997).

(2) The influence of the close background thermal emission is strong and can hardly be taken into account in a priori performance estimations.

5. First Binary Images and SEDs

The detailed data reduction is in progress; some preliminary results have been published by Monin et al. (1997) and the complete results, together with a deeper analysis of our data will be pub-

lished in a forthcoming paper. We present here some of the images after global reduction process, including the fit of the background baseline, but without any deconvolution applied (see Figure 5). Our background fitting procedure is equivalent to the spectral baseline fitting and removal in radio line observations, and we did use the dedicated CLASS package, developed at Grenoble Observatory and IRAM, for this purpose.

Note that we have not yet co-added all the available frames so that the signal-to-noise ratio can be upgraded in some images, especially the ones where the secondary is about ten times fainter than the primary.

We have also obtained detailed SEDs for the first time in the $1\text{--}5 \mu\text{m}$ range for both components on close binary systems. We show one example of such results in Figure 6.

Most of our objects have never been observed separately in the visible range. Still, in some cases, when the luminosity difference is large enough between both components, we attributed the visible magnitude value to the brighter one (i.e. the primary). Then we fitted a blackbody curve and a common visual absorption to the SEDs of both components, assuming interstellar characteristics for the dependence of the absorption on wavelength (this was the case for the SR9 system shown in Figure 6). Another possibility is to fit a blackbody to the J, H and K SED points of the fainter component, and to subtract the corresponding (fitted) V, R and I flux contribution from the primary (brighter) component, before fitting this latter SED from R to H (this was the case for the WSB20 system, where both components have identical flux to within a factor of two in the range F to K).

In the case shown in Figure 6 (SR9), the components of the binary can be ap-

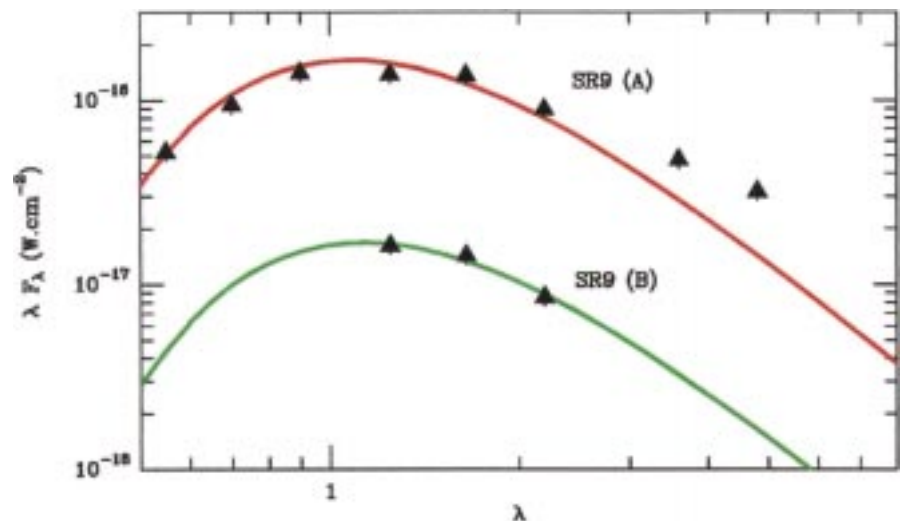


Figure 6: Spectral Energy Distribution of the components of the binary system SR9 (full triangles) together with their corresponding fitted blackbody curves (see text for details).

proximately described by the respective parameters: $L_A = 2.5 L_\odot$, $T_A = 3900$ K, $A_V = 0.9$ (same value for both components), $L_B = 0.25 L_\odot$, $T_B = 3800$ K. There appears to be an infrared excess over a blackbody photosphere on the primary component of SR9, indicating the presence of a probable accretion disk. This example illustrates the advantage of a high angular resolution 3–5 μm imaging detector.

6. Conclusion

We have used ADONIS + SHARP / COMIC to determine the SED of close PMS binaries in the full 1–5 μm range. This new instrument available at the 3.6-m telescope at ESO is very well suited for such scientific programmes. We have used this result to determine the physical characteristics of both components of these close binaries. To take full advantage of the 3–5 μm window on ADONIS + COMIC would require beam-switching

observations, but this is not possible with the current ADONIS setting. We therefore recommend to calibrate the close background emission by measuring it regularly (less than every hour or so) on a sky position empty of sources close to the object position. This appears particularly important if one wishes to observe extended sources like galaxies. The SED fitting procedure provides an approximate value for the visual absorption and the effective temperature. The access of the COMIC instrument to the 3–5 μm window will allow us to detect the presence of accretion disks around close binary components and study the relation of these disks with separation. A more precise determination of the spectral type of our binary targets will await the availability of the *GraF* adaptive optics infrared spectrometer currently under tests at ESO.

Acknowledgements. The adaptive optics observations would not have

been possible without the constant help and support of the ESO ADONIS team, and we are happy to thank here the ESO ADONIS team for its great help and enthusiasm during the run. Hervé Geoffroy acknowledges one year of ESO studentship during which this study has been performed.

References

- Devillard, N., 1997, *The Messenger*, **87**, 19.
 Ghez et al. 1993, *AJ*, **106**, 200.
 Herbig, G.H., and Bell, K.R., 1988, *Third Catalog of Emission-Line Stars of the Orion Population*, Lick Observatory Bulletin series.
 Lacombe et al., 1997, submitted.
 Leinert et al. 1993, *A&A*, **278**, 12.
 Marco et al., 1997, submitted.
 Monin et al., 1997, in *Poster Proceedings of IAU Symp. No. 182*, eds. Malbet & Castets, (1997), p. 230.
 Reipurth & Zinnecker, 1993. *A&A*. **278**, 81.

E-mail address:

Jean-Louis.Monin.@obs.ujf-grenoble.fr

An ESO 3.6-m/Adaptive Optics Search for Young Brown Dwarfs and Giant Planets

W. BRANDNER¹, J.M. ALCALÁ², S. FRINK³, and M. KUNKEL⁴

¹University of Illinois at Urbana-Champaign, USA

²Osservatorio Astronomico di Capodimonte, Napoli, Italy

³Astronomisches Rechen-Institut Heidelberg, Germany

⁴Max-Planck-Institut für Astronomie, Heidelberg, Germany

1. Extrasolar Planets and the Brown Dwarf Gliese 229 B

Only two years ago, the century-old paradigm that other planetary systems would be similar to our own solar system started to change. The discovery of extrasolar giant planets and brown dwarfs by monitoring radial velocities of nearby stars revealed that giant planets are not necessarily 5 to 30 AU away from their sun but may orbit at much smaller ($\ll 1$ AU) separations (Mayor & Queloz, 1995, Marcy & Butler, 1996).

While radial velocity surveys are most successful for discovering close companions, direct imaging allows one to probe systems with larger separations for which radial velocity methods are not sensitive. Indeed, Gl 229B, the first brown dwarf to be identified unambiguously, has a separation of 45 AU from the central star. It was discovered with an adaptive optics coronagraph at the Palomar 1.5-m telescope (Nakajima et al., 1995, Oppenheimer et al., 1995). Direct imaging of resolved objects also allows one to study their spectral features in detail.

As inferred by Allard & Hauschildt (1995) from computations of model at-

mospheres, the energy distribution of late-type dwarfs (and thus of young brown dwarfs and giant planets) is very peculiar. The molecular opacities that globally define the continuum cause the spectral energy distribution to peak around 1.1 μm for solar metallicities, almost independently of the effective temperature.

In Figure 1 we show on top a low-resolution spectrum of Gl 229 B (Oppenheimer et al., 1995). Below, adaptive optics images obtained with ADONIS/SHARP and the circular variable filter ($\lambda/\Delta\lambda \approx 60$) at three distinct wavelength bands on and off molecular absorption bands are shown. The image scale was 0.035"/pixel. Four two-minute exposures were coadded for each frame. No image deconvolution has been applied.

2. The Luminosity Evolution of Young Brown Dwarfs and Giant Planets

Younger brown dwarfs will have a higher luminosity, their bolometric luminosity L_{BD} evolves with time t as $L_{BD} \propto t^{-1.2}$ (Black, 1980, Burrows et al., 1995¹) Pre-main-sequence stars exhibit a tem-

poral luminosity evolution similar to brown dwarfs. However, their luminosity L_{PMS} decreases much slower than that of brown dwarfs (e.g. $L_{PMS} \propto t^{-0.7}$ for a pre-main-sequence star with a mass of 0.5 M_\odot and an age between 10^5 and 10^8 yr, D'Antona & Mazzitelli, 1994).

Figure 2 illustrates the evolution of the luminosity ratio of a 0.02 M_\odot brown dwarf and a 0.50 M_\odot star. Whereas at an age of 10^6 yr to 10^7 yr the luminosity ratio is in the range of ≈ 0.1 to 0.03, it will be two orders of magnitude smaller at an age of 10^9 yr. It will become increasingly harder to detect a brown dwarf next to an "older" pre-main-sequence star or even a main-sequence star than next to a young pre-main-sequence star – always assuming that the star and the brown dwarf are coeval. Studies of the individual components of pre-main-sequence binaries revealed that most of them are indeed coeval (Hartigan et al., 1994, Brandner & Zinnecker, 1997).

Because of the smaller brightness difference, it should be much easier to de-

¹Note that these calculations did not consider the fact that brown dwarfs with masses $\geq 13 M_{\text{Jupiter}}$ will start Deuterium burning and might be considerably brighter over a short period of time.